Carrier-Frequency-Offset (CFO)-aware Deep Learning-based Orthogonal Frequency-Division Multiplexing (OFDM) Detection under a 60 GHz Clustered Delay Line Channel

Noever Q. Saile [1] and Lawrence Materum [1,2,*]

[1] Department of Electronics, Computer, and Electrical Engineering, De La Salle University, Manila, 1004, Philippines
[2] International Centre, Tokyo City University, Tokyo, 158-8557, Japan
Email: noever_saile@dlsu.edu.ph (N.Q.S.); materuml@dlsu.edu.ph (L.M.)
*Corresponding author

***Abstract*—This paper evaluates classical, end-to-end deep learning, and hybrid Orthogonal Frequency-Division Multiplexing (OFDM) receivers under a 60 GHz Third-Generation Partnership Project Technical Report 38.901 Clustered Delay Line Model A (3GPP TR 38.901 CDL-A) channel with explicit synchronization impairments. Four receivers are compared: no equalization, pilot-assisted least-squares channel estimation with Least-Squares Zero-Forcing (LS-ZF), an end-to-end regression Deep Neural Network (DNN), and a hybrid Least-Squares-aided Deep Neural Network (LS-DNN) detector. The main contribution is a Carrier-Frequency-Offset (CFO)-aware comparison of whether a simple fully connected DNN is more effective as a direct receiver replacement or as a post-equalization refinement stage. The impairment model includes frame-wise common phase error and deterministic normalized CFO. Performance is evaluated from 0−50 dB using Bit Error Rate (BER), symbol Mean Squared Error (MSE), Error Vector Magnitude (EVM), receiver runtime, and Wilson confidence intervals over $\epsilon \in \{0, 0.01, 0.02, 0.05, 0.06, 0.10\}$. Results indicate that LS-ZF remains the strongest BER baseline, while the hybrid detector is BER-competitive at low-to-moderate CFO and improves symbol-fidelity metrics in several CFO-impaired cases. At $\epsilon = 0.10$, all receivers degrade sharply, showing limited robustness outside the DNN CFO training range. Overall, the results suggest that deep learning is more useful as a structured post-equalization refinement stage than as a universal end-to-end OFDM receiver replacement.**

***Keywords*—Orthogonal Frequency Division Multiplexing (OFDM), deep learning, carrier frequency offset, clustered delay line channel, hybrid receiver, millimeter wave, signal detection**

I. Introduction

Orthogonal Frequency Division Multiplexing (OFDM) remains a core waveform for broadband wireless systems because of its efficient implementation and robustness to multipath propagation [1]. However, OFDM performance depends strongly on accurate channel estimation and synchronization. Residual Carrier Frequency Offset (CFO), Common Phase Error (CPE), and related phase distortions degrade OFDM performance. They destroy subcarrier orthogonality, introduce Inter-Carrier Interference (ICI), and affect both bit decisions and constellation quality [2–4]. These effects become increasingly important in high-frequency systems, including millimeter wave (mmWave) links, where oscillator and propagation constraints are more severe [5, 6].

For channel-aware OFDM detection, classical receivers typically rely on pilot-assisted estimation followed by linear equalization. In many practical settings, Least-Squares (LS) and related model-based equalization methods remain strong baselines because they are simple, interpretable, and effective when the assumed signal model is sufficiently accurate. At the same time, their performance can degrade when impairments such as CFO or phase instability violate the ideal one-tap-per-subcarrier assumption.

Deep learning has also emerged as an alternative approach for physical-layer signal processing by learning nonlinear mappings directly from received samples or structured receiver features [7, 8]. Early work showed that neural networks can be used for OFDM channel estimation and detection. Later studies, however, suggested that model-driven and hybrid receivers may be more robust than purely black-box designs, especially in challenging operating regimes [9–15].

Despite this progress, an important evaluation gap remains. Deep learning has already been studied under 5G-compliant and model-driven receiver settings, including more advanced convolutional and hybrid designs. However, less is known about how the simpler fully connected regression architecture introduced by

Manuscript received April 13, 2026; revised May 27, 2026; accepted June 30, 2026; published September 18, 2026.

Ye *et al.* [10] behaves when used in two different roles under the same standardized mmWave channel, as a raw-feature E2E detector and as a post-equalization hybrid correction stage. This distinction is important because a learned detector may perform very differently depending on whether it must learn the entire receiver mapping or only refine a model-based equalized signal.

This work addresses that gap by evaluating four receiver configurations under the Third-Generation Partnership Project Technical Report 38.901, Clustered Delay Line Model A (3GPP TR 38.901 CDL-A) channel at 60 GHz: No Equalization (NoEQ), classical Least-Squares Zero-Forcing (LS-ZF), an End-to-End (E2E) regression DNN, and a hybrid Least Squares + Deep Neural Network (LS + DNN) detector. Unlike end-to-end replacements that discard receiver structure, the hybrid approach preserves a pilot-assisted LS front-end and applies deep learning only as a nonlinear correction stage. This design choice is motivated by the broader model-driven deep learning literature, which argues that incorporating communication-domain structure can improve interpretability, reduce training burden, and enhance robustness [11, 13].

The main contributions of this paper are as follows. First, it presents a CFO-aware OFDM receiver evaluation under the standardized 3GPP TR 38.901 CDL-A channel at 60 GHz with explicit frame-wise CPE and deterministic normalized CFO. Second, it compares a raw-feature E2E regression DNN against a structured hybrid LS + DNN detector using the same fully connected architecture introduced by Ye *et al.* [10]. Third, it evaluates the detectors not only in terms of Bit Error Rate (BER), but also in symbol Mean Squared Error (MSE), Error Vector Magnitude (EVM), offline training behavior, receiver runtime, and Monte Carlo confidence intervals over an expanded CFO sweep. Fourth, it positions the resulting performance against existing solution families in the literature, classical pilot-assisted equalization, fully data-driven OFDM detectors, and model-driven hybrid receivers.

Overall, this study examines whether, under a standardized 3GPP mmWave setting with explicit phase-related impairment, deep learning is more useful as a direct receiver replacement or as a structured refinement stage.

II. Literature Review

A. Classical OFDM Impairments and Their Relevance to mmWave

Synchronization errors are a well-established source of OFDM degradation. CFO and phase noise break subcarrier orthogonality, introduce inter-carrier interference, and increase BER by affecting both hard symbol decisions and constellation quality [1–4]. These effects become more important in high-frequency systems because oscillator impairments and propagation constraints are more pronounced at mmWave bands [5, 6]. For this reason, the 3GPP TR 38.901 CDL channel model provides a more realistic basis for receiver evaluation than simplified fading models, particularly for frequencies up to 100 GHz [16].

Recent studies have also considered learning-based CFO estimation and synchronization in OFDM and 5G-related settings. Wang *et al.* [17] evaluated deep-learning-based CFO estimation across multiple channel models, while more recent Tracking Reference Signal (TRS) and Cell Reference Signal (CRS)-based approaches studied CFO and channel estimation in 5G and vehicular OFDM systems [18, 19]. These works are complementary to the present study because they mainly estimate or correct CFO. In contrast, this paper evaluates how different detector roles behave when a deterministic normalized CFO remains present in the received signal.

B. Deep Learning for OFDM Detection and Channel Estimation

Deep learning has been widely studied for physical-layer communication tasks, including end-to-end learning, channel estimation, and signal detection [7–9]. In OFDM, Ye *et al.* [10] showed that a fully connected regression DNN can be used for channel estimation and data detection. Later works extended this direction through deep channel estimation, joint channel estimation and detection, and receiver designs for hardware-impaired OFDM systems [20–22].

However, the literature also shows that purely data-driven receivers are not always the most robust option. Model-driven approaches combine communication-domain structure with learnable modules to improve interpretability and robustness [13, 23]. The Combination of Deep Learning and Expert Knowledge in OFDM Receivers (ComNet) architecture demonstrated the benefit of combining conventional OFDM receiver structure with DNN refinement, while the Fully Convolutional Deep Learning Receiver (DeepRx) showed the strength of fully convolutional learned receivers in richer 5G-compliant settings [11, 12]. Related studies on power-efficient learned receivers and comparative evaluations of deep and iterative methods further show that performance depends strongly on Signal-to-Noise Ratio (SNR), impairment type, receiver structure, and deployment constraints [14, 15, 24, 25].

C. Positioning of the Present Study

The present work is positioned within this model-driven receiver trend, but it deliberately retains the simpler fully connected architecture introduced by Ye *et al.* [10]. Unlike ComNet or DeepRx, the aim is not to propose a new state-of-the-art neural receiver, but to examine where a simple DNN is more effective under a standardized mmWave channel with explicit phase-related impairments. This position allows the study to compare the same DNN architecture in two roles: as a raw-feature E2E detector and as a hybrid LS-assisted post-equalization correction stage.

The main distinctions of this work are therefore fourfold. First, it uses the standardized 3GPP TR 38.901 CDL-A channel at 60 GHz instead of only simplified fading channels. Second, it explicitly includes frame-wise CPE and deterministic normalized CFO through a time-domain phase ramp. Third, it compares End-to-End (E2E) and hybrid DNN roles under the same fully connected architecture. Fourth, it evaluates BER together with symbol MSE and EVM, which helps reveal residual constellation distortion that may not always appear as a BER difference. This framing avoids treating the learned receiver as a guaranteed replacement for classical OFDM detection and instead evaluates whether learning is more useful as a direct detector or as a structured refinement stage [11, 13, 14].

III. Materials and Methods

A. System Overview

The evaluated receiver chain follows a conventional OFDM physical-layer flow under the 3GPP TR 38.901 CDL-A channel at 60 GHz, with explicit phase-related impairments and four receiver configurations: (i) classical detection without equalization (NoEQ), (ii) classical pilot-assisted LS-ZF equalization, (iii) an E2E regression DNN operating on raw received frequency-domain OFDM symbols, and (iv) a hybrid LS + DNN detector that applies deep learning as a nonlinear correction stage after LS equalization. Each frame contains two OFDM symbols (1 pilot + 1 data), preserving compatibility with the regression architecture introduced by Ye *et al.* [10] and the fixed 256-dimensional DNN input used in this study. Training data are generated using the same standardized CDL-A channel and impairment model used during testing. Two separate DNN models are trained: one for the E2E feature representation and one for the hybrid LS-assisted feature representation. Testing is performed over a 0–50 dB Signal-to-Noise Ratio (SNR) sweep and an expanded normalized-CFO set $\epsilon \in \{0, 0.01, 0.02, 0.05, 0.06, 0.10\}$, with the detailed evaluation procedure described in Section III-H.

B. OFDM Frame Structure and TR 38.901 CDL Channel

An OFDM frame contains one block-type pilot symbol and one data symbol (frame size of 2). Quadrature Phase-Shift Keying (QPSK) modulation ($M = 4$) is applied to 63 active subcarriers, and a DC null is inserted for an Inverse Fast Fourier Transform (IFFT)/Fast Fourier Transform (FFT) size of $N_{\text{FFT}} = 64$. A Cyclic Prefix (CP) of length $N_{\text{CP}} = 16$ is appended. Let $x[n]$ denote the transmitted time-domain OFDM signal including CP. The 3GPP TR 38.901 CDL-A channel generates the noiseless received sequence:

$$r_0[n] = \sum_{\ell=0}^{L_h-1} h[\ell]\, x[n-\ell] \tag{1}$$

where $h[\ell]$ is the discrete-time multipath impulse response for the current channel realization and L_h is the number of discrete channel taps.

The CDL-A configuration used in both training and testing follows the MATLAB New Radio Clustered Delay Line channel (nrCDLChannel) System object with delay profile CDL-A, delay spread 30 ns, carrier frequency 60 GHz, sample rate 20 MHz, single-input single-output operation, path-gain normalization, output normalization, and zero Doppler shift. The maximum Doppler shift was fixed at 0 Hz to isolate multipath and synchronization effects from time-selective fading. Under nonzero Doppler, the channel would vary across frames and potentially within longer packet structures, which may reduce the reliability of pilot-assisted LS-ZF equalization and may require the DNN-based receivers to learn time-selective channel behavior in addition to CFO-induced distortion. Therefore, nonzero-Doppler evaluation is expected to affect the absolute error rates and may increase the value of model-driven temporal architectures. However, it is not expected to change the central interpretation that the hybrid detector benefits from retaining the receiver structure.

C. Time-Domain Impairments: Common Phase Error and Normalized CFO

After channel filtering, two phase-related impairments are applied in the time domain.

A random Common Phase Error (CPE) is drawn once per OFDM frame and applied identically to both OFDM symbols (pilot and data), including their cyclic prefixes:

$$r_1[n] = r_0[n] \exp(j\phi) \tag{2}$$

With $\phi \sim \mathcal{U}[-\phi_{\max}, +\phi_{\max}]$ and $\phi_{\max} = 10°$. These models residual frame-wise phase rotation in degrees while preserving the two-symbol frame structure used by the regression-based receiver. It should not be interpreted as a Wiener phase-noise process.

Normalized Carrier Frequency Offset (CFO) is modeled as a deterministic phase ramp:

$$r[n] = r_1[n] \exp\left(j2\pi \frac{\epsilon}{N_{\text{FFT}}} n\right) \tag{3}$$

where ϵ is the normalized CFO in subcarrier-spacing units, so that $\epsilon = 0.05$ corresponds to 5% of the subcarrier spacing, and $N_{\text{FFT}} = 64$. This deterministic complex exponential phase ramp is applied directly to the received time-domain samples, ensuring that the impairment magnitude is directly interpretable relative to OFDM subcarrier spacing.

Finally, AWGN is added to form the received sequence $y[n] = r[n] + w[n]$, where $w[n]$ is complex circular Gaussian noise. Combining channel and impairments yields:

$$y[n] = \left(\sum_{\ell=0}^{L_h-1} h\,[\ell] x[n-\ell]\right) \mathrm{e}^{j\phi} \mathrm{e}^{j2\pi \frac{\epsilon}{N_{\text{FFT}}} n} + w[n] \tag{4}$$

The present impairment model deliberately uses deterministic normalized CFO rather than stochastic Wiener phase noise. This choice was made to isolate the effect of a controllable frequency mismatch on the four receiver roles and to make the CFO severity directly interpretable in subcarrier-spacing units. A Wiener phase-noise process would introduce additional oscillator-memory effects and time-correlated random phase drift, making it more difficult to separate CFO sensitivity from stochastic phase-noise tracking behavior.

Therefore, stochastic phase noise is treated as a separate extension rather than being combined with the deterministic CFO sweep in the present evaluation.

D. OFDM Receiver Processing and Pilot-based Phase Compensation

The receiver removes the cyclic prefix and applies Fast Fourier Transform (FFT) to obtain the frequency-domain symbols. Since the frame-wise common phase error applies a common rotation to the pilot and data symbols within a frame, a pilot-based phase compensation step is used to reduce this common phase error. Let $R_p[k]$ be the received pilot tone on subcarrier k, and $X_p[k]$ the known pilot value. The phase estimate is:

$$\hat{\phi} = \angle\left(\frac{1}{|\mathcal{P}|}\sum_{k\in\mathcal{P}} R_p\,[k]\overline{X_p[k]}\right) \tag{5}$$

where $\mathcal{P}$ denotes the set of pilot subcarriers. All received subcarriers are then rotated by $\mathrm{e}^{-j\hat{\phi}}$. This step compensates for the dominant frame-wise CPE but does not remove CFO-induced Inter-Carrier Interference (ICI), which remains after FFT because CFO breaks subcarrier orthogonality.

E. Classical Reference Detectors

1) No Equalization (NoEQ)

The NoEQ receiver directly demodulates the received data subcarriers after FFT and pilot-based common-phase compensation, without any explicit channel equalization. This detector serves as a lower-bound reference illustrating the importance of equalization in frequency-selective fading channels.

2) Pilot-assisted LS-ZF equalization

The LS-ZF receiver estimates the channel response from the pilot symbol using:

$$\hat{H}_{\mathrm{LS}} = \frac{R_p}{X_p} \tag{6}$$

And applies one-tap zero-forcing equalization to the received data tones:

$$Y_{\mathrm{eq}} = \frac{R_d}{\hat{H}_{\mathrm{LS}}} \tag{7}$$

where R_d denotes the received data symbol in the frequency domain. After removing the DC subcarrier, the first $K = 8$ data tones are selected for evaluation. This choice follows the fixed-output regression setup introduced by Ye *et al*. [10], where the DNN predicts the real and imaginary components of eight QPSK data tones, producing a 16-dimensional regression target.

In implementation, a small floor of 10^{-12} is applied to $|\hat{H}_{\mathrm{LS}}|$ before division to avoid numerical overflow when an estimated channel coefficient is extremely close to zero.

Although an LMMSE-like shrinkage equalizer was also explored during preliminary experiments, the final reported four-way evaluation focuses on NoEQ and LS-ZF as the classical reference methods because the LMMSE-like and LS-ZF outputs were observed to be effectively identical under the reported setting.

F. DNN Feature Construction

This work evaluates two DNN input formulations using the same fully connected regression architecture.

End-to-End (E2E) Raw-Frame Feature: For the E2E model, the DNN input is formed directly from the raw received OFDM frame in the frequency domain after FFT and pilot-based phase compensation. Both OFDM symbols in the frame (pilot and data) are retained, including the DC component, producing a 64×2 complex array. The frame is then flattened in column-major order and converted into a 256-dimensional real vector by interleaving the real and imaginary parts of each complex element, yielding.

$$f_{\mathrm{E2E}} \in \mathbb{R}^{256} \tag{8}$$

This representation allows the DNN to learn a direct mapping from the received frame to the transmitted symbols without explicit channel equalization.

Hybrid LS + DNN Feature: For the hybrid model, the received pilot symbol is first used to estimate the channel response across the 64 FFT bins:

$$\hat{H}_{\mathrm{LS}} = \frac{R_p}{X_p} \tag{9}$$

The received data symbol is then LS-equalized using this estimate:

$$Y_{\mathrm{eq}} = \frac{R_d}{\hat{H}_{\mathrm{LS}}} \tag{10}$$

The hybrid DNN input is constructed from two structured complex-valued columns, the LS channel estimate $\hat{H}_{\mathrm{LS}}$ and the LS-equalized data symbol Y_{eq}. These form a 64×2 complex array:

$$U_{\mathrm{HYB}} = \left[\hat{H}_{\mathrm{LS}}, Y_{\mathrm{eq}}\right] \tag{11}$$

The DC row is retained for dimensional consistency but set to zero because the DC subcarrier is not transmitted. The array is then flattened and converted into a 256-dimensional real vector by interleaving the real and imaginary parts:

$$f_{\mathrm{HYB}} \in \mathbb{R}^{256} \tag{12}$$

Before being passed to the DNN, the real-valued hybrid feature entries are clipped to $[-10, 10]$ for numerical stability.

This construction preserves the same input dimensionality as the E2E model while exposing model-assisted information to the DNN. In this formulation, the DNN is not required to infer the channel response directly from the raw received frame; instead, it receives both the pilot-derived LS channel estimate and the corresponding LS-equalized data symbol.

For both DNNs, the regression target is the concatenated real and imaginary components of the transmitted QPSK symbols on the first $K = 8$ data tones, yielding a 16-dimensional output label.

G. DNN Architecture and Training Setup

Both DNN models follow the fully connected regression architecture introduced in Ref. [10], with input length 256, hidden-layer sizes 500, 250, and 120, and a 16-dimensional regression output. The fully connected architecture contains approximately 285,806 trainable parameters for each DNN model. The models were trained using the Root Mean Square Propagation (RMSProp) optimizer for 20 epochs using a mini-batch size of 10 and mean squared error loss.

The initial learning rate is 10^{-3} with a piecewise schedule that multiplies the learning rate by 0.8 every two epochs. L_2 regularization is set to 0.003, and validation is evaluated every 500 iterations.

Training data consist of 75,000 frames split into 80% training and 20% validation. The SNR for each training frame is randomly sampled from 0–50 dB in 5 dB steps to improve robustness across noise levels. Discrete 5 dB SNR levels follow the evaluation grid used in the reported Bit Error Rate (BER), Mean Squared Error (MSE), and Error Vector Magnitude (EVM) curves and keep training aligned with the tested operating points. A continuous uniform SNR distribution could further improve interpolation robustness between grid points and will be considered in future training designs. CFO augmentation is enabled during training, where the normalized CFO is sampled uniformly in $[-0.05, 0.05]$ per frame. Two separate models are trained: one using the E2E raw-frame feature representation and another using the structured hybrid feature formed from $\hat{H}_{\text{LS}}$ and the LS-equalized data symbol. This training phase yields the two trained models used in the final evaluation: one for the E2E feature representation and one for the structured hybrid LS-assisted feature representation.

H. Testing Procedure and Fixed-frame Monte Carlo Evaluation

Testing uses Monte Carlo simulation for SNR values from 0 to 50 dB in 5 dB steps and normalized CFO values:

$$\{0, 0.01, 0.02, 0.05, 0.06, 0.10\} \tag{13}$$

The CFO values $\epsilon = 0.01$, $\epsilon = 0.02$, and $\epsilon = 0.05$ lie within the DNN training augmentation range $[-0.05, 0.05]$. The value $\epsilon = 0.06$ is an extrapolation case, while $\epsilon = 0.10$ is an out-of-training-distribution stress case.

For AWGN generation, the specified SNR is adjusted by the active-subcarrier-to-FFT-size ratio as Eq. (14):

$$\text{SNR}_{\text{OFDM}} = \text{SNR} + 10\log_{10}\left(\frac{63}{64}\right) \tag{14}$$

which accounts for the 63 active subcarriers and one Direct-Current (DC) null in the 64-point FFT.

For each SNR–CFO condition, 100,000 shared frames are generated before detector-specific evaluation. Each shared frame contains the transmitted bits and QPSK symbols, pilot insertion, OFDM modulation, CDL-A channel realization, frame-wise CPE, normalized CFO, AWGN realization, FFT output, and pilot-based phase-compensated received frame. The same shared frame is then passed to all four receiver variants. This frame ensures that NoEQ, LS-ZF, E2E DNN, and Hybrid LS + DNN are evaluated using identical transmitted bits, channel realization, CPE, CFO, and noise realization for each frame index. The fixed value of 100,000 frames was chosen to avoid the excessive runtime and reproducibility concerns of adaptive high-SNR stopping rules while still providing a large and uniform Monte Carlo sample across all SNR-CFO conditions. Since each frame evaluates $K = 8$ QPSK symbols, each detector is evaluated over 1.6×10^6 transmitted bits per SNR-CFO condition.

Detector evaluation is performed only after the shared received frame has been generated. The NoEQ and LS-ZF receivers are evaluated frame by frame from the shared received frame. For the E2E and hybrid DNN receivers, the corresponding feature vectors are first collected across all frames and then evaluated using batched DNN inference to reduce prediction overhead. Shared frame-generation time is reported separately from receiver runtime. Therefore, the reported receiver runtime reflects detector-side processing only, including feature construction, DNN inference where applicable, and output scoring.

Wilson 95% confidence intervals are reported for BER. Frame-wise MSE variability is also computed during evaluation and used to support the interpretation of symbol-level trends.

I. Simulation Parameters

Table I summarizes the simulation settings used throughout training and testing.

TABLE I. SIMULATION AND TRAINING PARAMETERS

Parameter	Value
Carrier frequency	60 GHz
Channel model	TR 38.901 CDL-A
MATLAB channel object	nrCDLChannel
Sample rate	20 MHz
Delay spread	30 ns
Doppler shift	0 Hz
FFT size (N_{FFT})	64
Active subcarriers	63, with DC null inserted
CP length (N_{CP})	16
Frame structure	1 pilot symbol + 1 data symbol
Pilot value	$1 - j$
Modulation	QPSK
CPE range	$\phi \sim \mathcal{U}[-10°, 10°]$
CFO test cases	$\epsilon = 0, 0.01, 0.02, 0.05, 0.06, 0.10$
Training SNR set	0, 5, 50 dB, random per frame
Training frames per DNN	75,000, with 80/20 training-validation split
Trained DNNs	E2E and Hybrid LS + DNN
Optimizer	RMSProp, 20 epochs, batch size 10
Initial learning rate	10^{-3}
Learning-rate schedule	Piecewise, drop factor 0.8 every 2 epochs
L2 regularization	0.003
Validation frequency	Every 500 iterations

Parameter	Value
Test frames per SNR–CFO case	100,000
Runtime reporting	Shared frame generation separated from receiver runtime
Detected/evaluated tones	K = 8, first 8 data tones

J. Performance Metrics

Symbol MSE is computed as Eq. (15).

$$\mathrm{MSE} = \mathbb{E}\left\{\left|X - \hat{X}\right|^2\right\} \tag{15}$$

BER is calculated as Eq. (16).

$$\mathrm{BER} = \frac{N_{\mathrm{bit,err}}}{N_{\mathrm{bit,total}}} \tag{16}$$

For BER, 95% confidence intervals are computed using the Wilson score interval:

$$\hat{p}_{\mathrm{W}} = \frac{\hat{p}+\frac{z^2}{2N}}{1+\frac{z^2}{N}} \tag{17}$$

$$\Delta_{\mathrm{W}} = \frac{z}{1+\frac{z^2}{N}}\sqrt{\frac{\hat{p}(1-\hat{p})}{N}+\frac{z^2}{4N^2}} \tag{18}$$

where $\hat{p} = \frac{N_{\mathrm{bit,err}}}{N_{\mathrm{bit,total}}}$, $N = N_{\mathrm{bit,total}}$, and $z = 1.96$ for a 95% interval. The interval is then $\hat{p}_{\mathrm{W}} \pm \Delta_{\mathrm{W}}$. EVM (RMS, normalized) is:

$$\mathrm{EVM} = \sqrt{\frac{\mathbb{E}\left\{\left|X-\hat{X}\right|^2\right\}}{\mathbb{E}\{|X|^2\}}} \times 100\% \tag{19}$$

For consistency across the four reported detectors, all metrics are computed on the same detected scope: the first $K = 8$ data tones of the OFDM data symbol. This scope ensures direct comparability among NoEQ, LS-ZF, E2E DNN, and Hybrid LS + DNN.

IV. Result and Discussion

This section presents detector performance under the 3GPP TR 38.901 CDL-A channel at $f_c = 60$ GHz across the expanded normalized-CFO sweep $\epsilon \in \{0, 0.01, 0.02, 0.05, 0.06, 0.10\}$. In addition to BER, symbol MSE, and EVM, it reports receiver runtime, offline training behavior, and confidence intervals.

A. Offline Training Behavior and Convergence

Both DNN models were trained locally in MATLAB R2025b Update 3 on a laptop equipped with an NVIDIA GeForce RTX 4060 Laptop GPU. The E2E and hybrid models both completed the full 20 training epochs with the status Max epochs completed, confirming stable training without early failure or divergence.

The E2E model required a wall-clock training time of 1835.62 s (30.59 min), while the hybrid model required 1633.91 s (27.23 min). Thus, the hybrid model was slightly faster to train offline. The final reported validation Root Mean Square Error (RMSE) was 1.3813 for the E2E model and 1.4964 for the hybrid model. Despite the slightly lower validation RMSE of the E2E model, its final communication performance in BER, MSE, and EVM was generally worse than that of LS-ZF and the hybrid detector at moderate-to-high SNR. This result shows that lower validation regression loss does not necessarily produce better hard-decision detection under the evaluated channel and impairment conditions.

The training-progress plots also show smooth convergence, with the largest loss reduction occurring early in training and later epochs producing more gradual improvement.

B. Receiver Runtime

Fig. 1 shows receiver runtime per SNR point for the expanded CFO sweep, while Fig. 2 summarizes total receiver runtime across the SNR sweep for each CFO value.

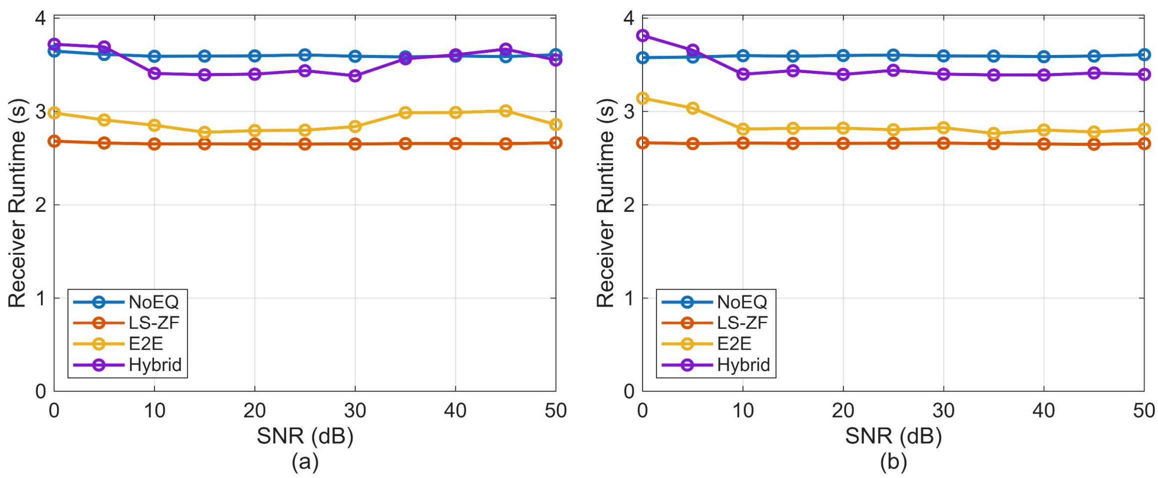

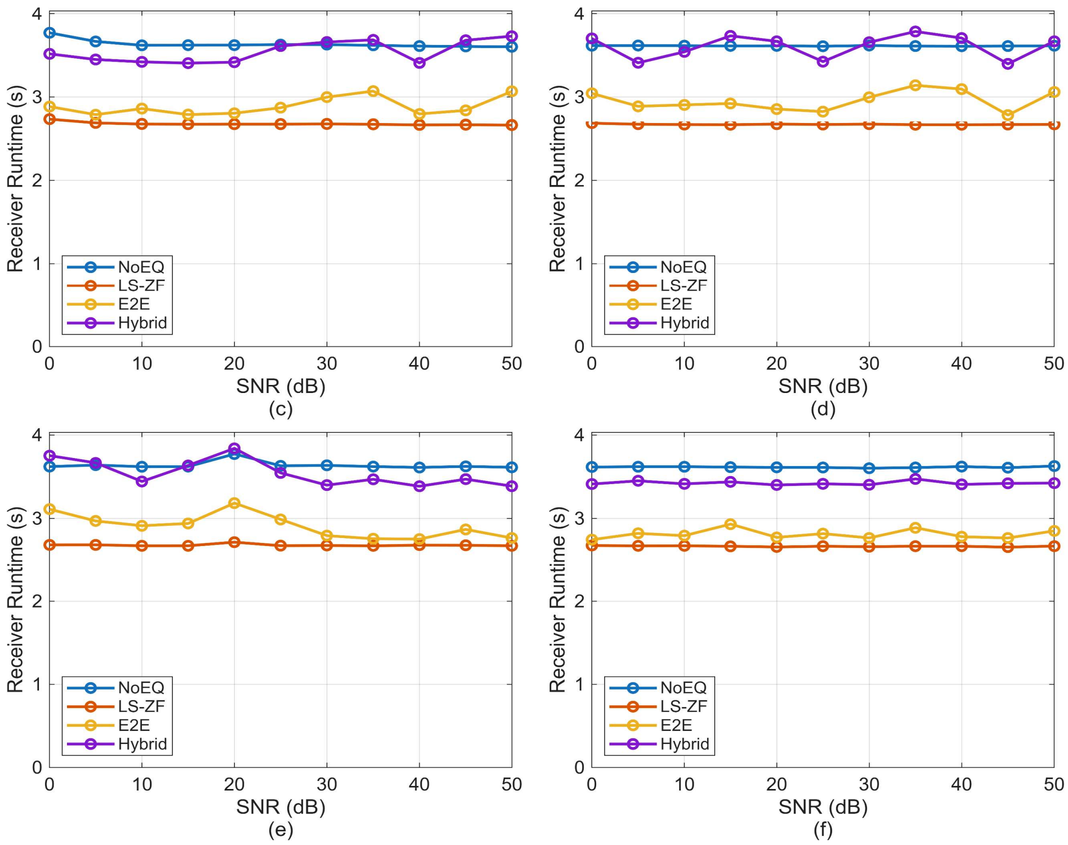

Fig. 1. Receiver runtime per SNR point for six normalized CFO values: (a) $\epsilon = 0$, (b) $\epsilon = 0.01$, (c) $\epsilon = 0.02$, (d) $\epsilon = 0.05$, (e) $\epsilon = 0.06$, and (f) $\epsilon = 0.10$.

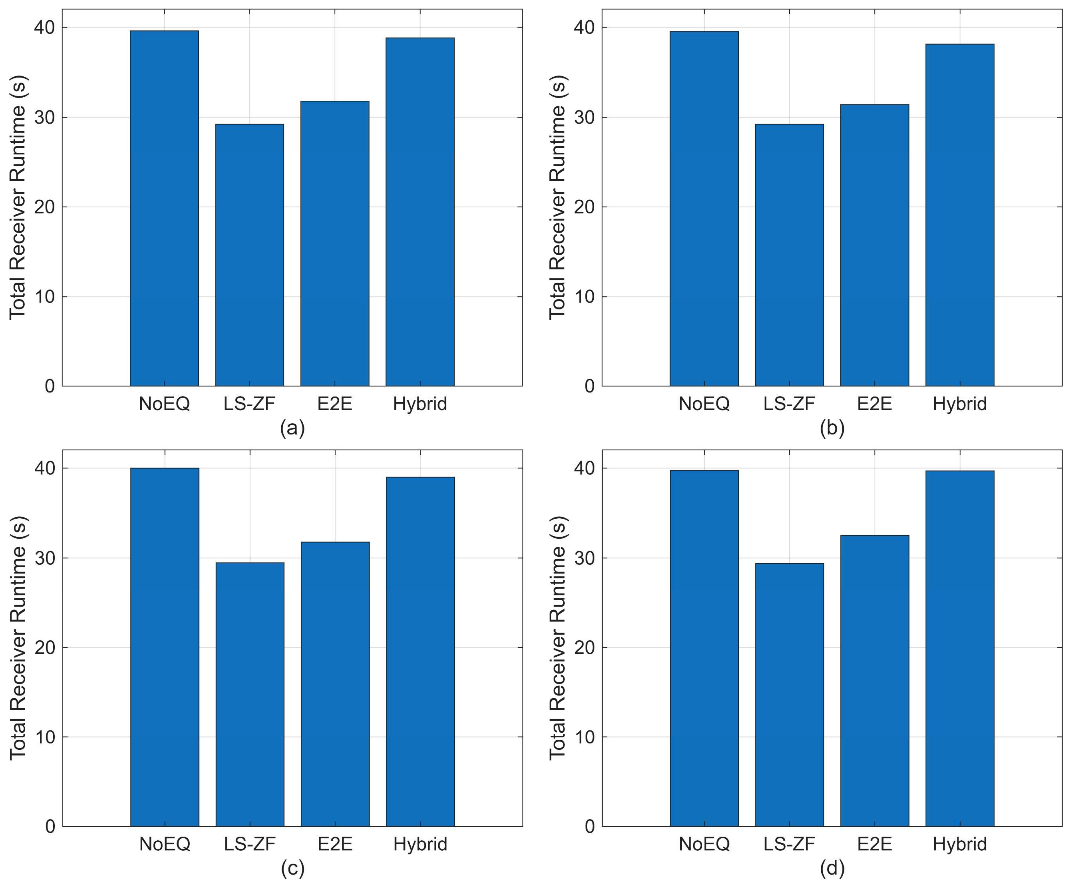

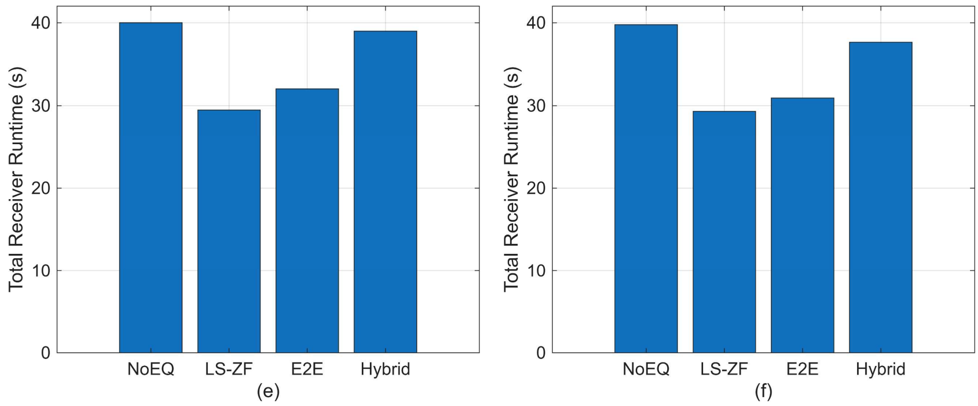

Fig. 2. Total receiver runtime across the SNR sweep for six normalized CFO values: (a) $\epsilon = 0$, (b) $\epsilon = 0.01$, (c) $\epsilon = 0.02$, (d) $\epsilon = 0.05$, (e) $\epsilon = 0.06$, and (f) $\epsilon = 0.10$.

Because all detectors are evaluated using the same number of frames per SNR-CFO condition, runtime differences primarily reflect receiver-side processing rather than unequal Monte Carlo stopping behavior. The shared frame-generation stage is executed once per frame. It includes bit generation, OFDM modulation, CDL-A channel filtering, CPE/CFO impairment injection, AWGN addition, FFT processing, and pilot-based phase compensation. This shared stage is not attributed to any individual detector.

For the six CFO values reported in the manuscript, the accumulated shared frame-generation time was approximately 4.27×10^4 s. By contrast, the receiver-side runtimes across the same reported CFO sweep were much smaller, 238.68 s for NoEQ, 176.11 s for LS-ZF, 190.47 s for E2E, and 232.30 s for Hybrid. Thus, the total wall-clock simulation cost is dominated by shared signal generation, while the detector-side runtime differences remain comparatively small. The classical receivers generally require the lowest receiver-side runtime, while the DNN-based receivers incur additional cost from feature construction and neural-network inference. Nevertheless, the hybrid receiver remains in the same practical runtime range as the other evaluated detectors.

C. *Computational Complexity and Inference Scalability*

The computational burden of the evaluated receivers differs mainly in the detector stage. NoEQ has the lowest detector-side complexity because it performs direct demodulation after FFT and phase compensation. LS-ZF adds pilot-based channel estimation and one complex division per evaluated subcarrier, giving a lightweight model-based baseline. The E2E and hybrid DNN receivers add feedforward neural-network inference after feature construction. For the fully connected architecture used in this study, the dominant inference cost comes from the dense layers with sizes 256–500–250–120–16, corresponding to approximately 2.85×10^5 trainable parameters per DNN. This architecture is substantially simpler than convolutional or model-driven receiver families such as DeepRx- or ComNet-like architectures, which can exploit richer time-frequency structure but generally require more specialized architectural design and implementation. In the present results, the DNN-based receivers incur higher detector-side processing than LS-ZF, but the measured runtime remains in the same order of magnitude as the classical receivers. Therefore, the hybrid LS + DNN detector is best viewed as a moderate-complexity refinement stage rather than as a fully general high-capacity neural receiver.

D. *BER Performance Across CFO Values*

Fig. 3 reports BER versus SNR for the four receiver configurations across the reported CFO values.

Across the CFO sweep, NoEQ remains poor because detection without channel equalization is dominated by frequency-selective distortion. LS-ZF is the strongest BER baseline over most low-to-moderate CFO conditions. At 50 dB, LS-ZF reaches 1.06×10^{-5} for $\epsilon = 0$, 0 observed errors for $\epsilon = 0.01$, 8.13×10^{-6} for $\epsilon = 0.02$, and 3.06×10^{-5} for $\epsilon = 0.05$, as shown in Fig. 3(a)–(d), before degrading to 4.41×10^{-3} at $\epsilon = 0.06$ and 4.80×10^{-1} at $\epsilon = 0.10$, as shown in Fig. 3(e) and 3(f), respectively. The corresponding hybrid BER values are 1.00×10^{-5}, 6.25×10^{-7}, 8.75×10^{-6}, and 1.71×10^{-4}, respectively, increasing to 1.28×10^{-2} at $\epsilon = 0.06$ and 4.69×10^{-1} at $\epsilon = 0.10$. Thus, the hybrid detector remains close to LS-ZF at low CFO values but does not consistently improve BER.

The E2E detector exhibits a clearer high-SNR floor. At 50 dB, its BER remains 7.44×10^{-4} for $\epsilon = 0$ and increases to 2.53×10^{-3} at $\epsilon = 0.05$. This outcome confirms that the raw-feature E2E mapping is less reliable than the LS-ZF and hybrid approaches under the evaluated channel and impairment conditions.

The expanded CFO sweep also identifies the operating limit of the trained receivers. At $\epsilon = 0.06$, performance begins to degrade noticeably, especially for the DNN-based detectors, as shown in Fig. 3(e). At $\epsilon = 0.10$, which lies outside the training augmentation range $[-0.05, 0.05]$, all receivers collapse toward high BER values near random-decision behavior, as shown in Fig. 3(f). At 50 dB and $\epsilon = 0.10$, LS-ZF, E2E, and hybrid BER values are 4.80×10^{-1}, 4.55×10^{-1}, and 4.69×10^{-1}, respectively. These values indicate that the learned receivers should not be assumed to generalize to stronger CFO values without broader CFO training or explicit synchronization correction.

doi:10.12720/jcm.21.5.631-643

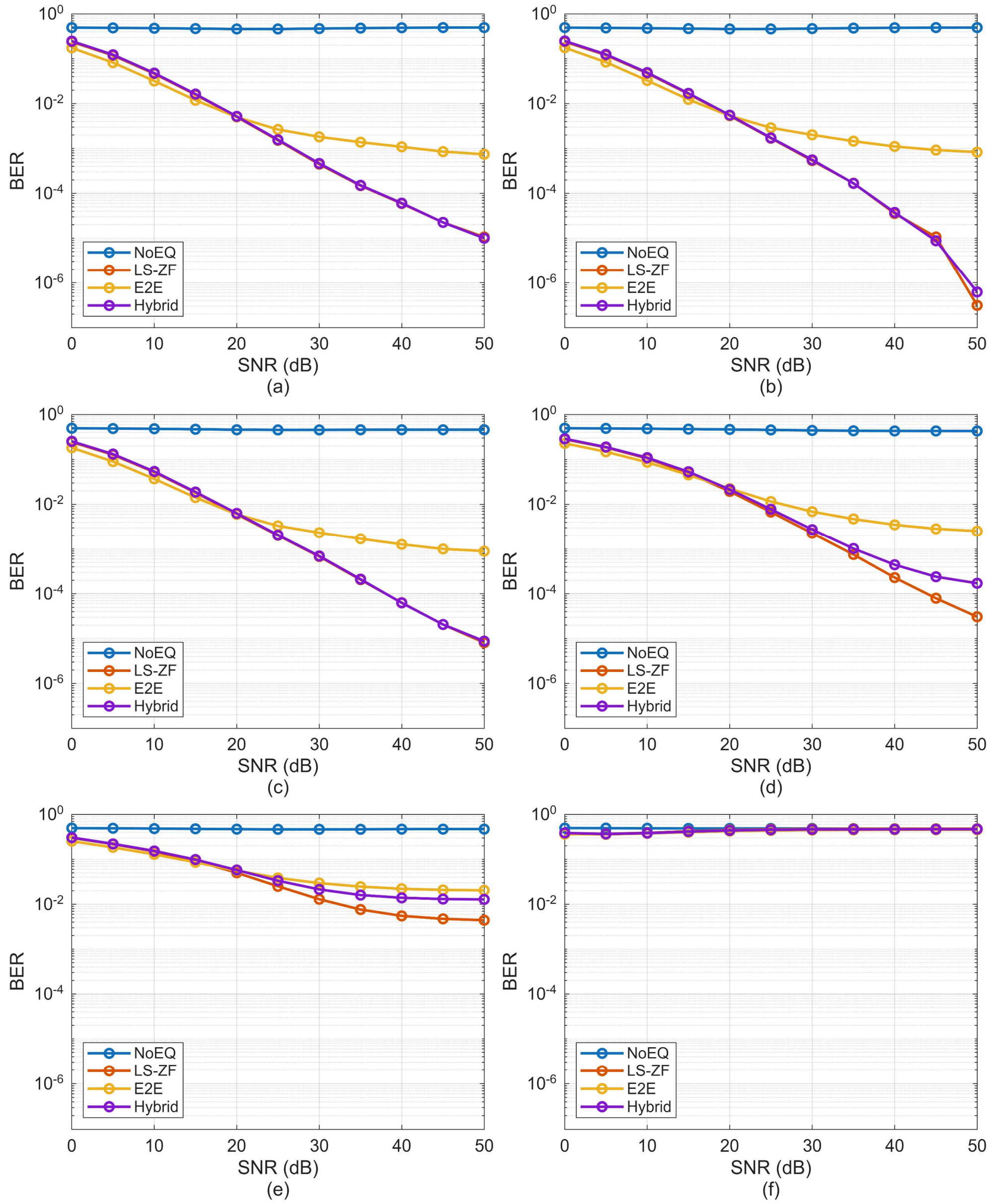

Fig. 3. BER versus SNR under the 3GPP TR 38.901 CDL-A channel at 60 GHz for six normalized CFO values: (a) $\epsilon = 0$, (b) $\epsilon = 0.01$, (c) $\epsilon = 0.02$, (d) $\epsilon = 0.05$, (e) $\epsilon = 0.06$, and (f) $\epsilon = 0.10$.

Table II reports the observed BER and 95% Wilson confidence intervals at 50 dB. A zero BER entry indicates that no bit errors were observed in the finite Monte Carlo sample; it should be interpreted through its upper confidence bound rather than as an absolute zero-error probability.

E. Symbol MSE: Residual Distortion Beyond BER

Fig. 4 shows symbol MSE versus SNR across the reported CFO values. Unlike BER, symbol MSE directly measures the average squared complex-symbol error and therefore captures residual amplitude and phase distortion even when hard decisions remain correct. This distinction is important because some receiver outputs remain on the correct side of the QPSK decision boundary while still exhibiting different constellation fidelity.

At low-to-moderate CFO values, the hybrid detector often reduces symbol distortion relative to the raw E2E detector and, in some conditions, relative to LS-ZF. At 50 dB and $\epsilon = 0.05$, LS-ZF obtains an MSE of 5.13×10^{-1}, while the hybrid detector obtains 4.04×10^{-2} as shown in Fig. 4(d). These values confirm that the hybrid DNN can reduce residual symbol-level distortion after LS equalization, even when the same gain does not translate into a BER improvement.

However, the MSE results also show that the CFO range bounds this benefit. At $\epsilon = 0.10$, all detectors exhibit large residual distortion, as shown in Fig. 4(f). This result supports the interpretation that the hybrid detector is useful as a post-equalization refinement stage within the trained CFO range, but not as a general solution for arbitrary CFO mismatch.

TABLE II. BER WITH 95% WILSON CONFIDENCE INTERVALS AT 50 DB ACROSS THE REPORTED CFO SWEEP

CFO ϵ	Detector	BER	95% CI Lower	95% CI Upper
0	NoEQ	4.979×10^{-1}	4.971×10^{-1}	4.987×10^{-1}
0	LS-ZF	1.063×10^{-5}	6.634×10^{-6}	1.702×10^{-5}
0	E2E	7.444×10^{-4}	7.033×10^{-4}	7.878×10^{-4}
0	Hybrid	1.000×10^{-5}	6.156×10^{-6}	1.625×10^{-5}
0.01	NoEQ	4.953×10^{-1}	4.946×10^{-1}	4.961×10^{-1}
0.01	LS-ZF	0	0	2.401×10^{-6}
0.01	E2E	8.338×10^{-4}	7.902×10^{-4}	8.797×10^{-4}
0.01	Hybrid	6.250×10^{-7}	1.103×10^{-7}	3.541×10^{-6}
0.02	NoEQ	4.588×10^{-1}	4.580×10^{-1}	4.596×10^{-1}
0.02	LS-ZF	8.125×10^{-6}	4.749×10^{-6}	1.390×10^{-5}
0.02	E2E	8.950×10^{-4}	8.498×10^{-4}	9.425×10^{-4}
0.02	Hybrid	8.750×10^{-6}	5.212×10^{-6}	1.469×10^{-5}
0.05	NoEQ	4.300×10^{-1}	4.292×10^{-1}	4.307×10^{-1}
0.05	LS-ZF	3.063×10^{-5}	2.317×10^{-5}	4.048×10^{-5}
0.05	E2E	2.531×10^{-3}	2.454×10^{-3}	2.610×10^{-3}
0.05	Hybrid	1.713×10^{-4}	1.521×10^{-4}	1.928×10^{-4}
0.06	NoEQ	4.724×10^{-1}	4.716×10^{-1}	4.731×10^{-1}
0.06	LS-ZF	4.409×10^{-3}	4.308×10^{-3}	4.513×10^{-3}
0.06	E2E	2.040×10^{-2}	2.018×10^{-2}	2.062×10^{-2}
0.06	Hybrid	1.279×10^{-2}	1.261×10^{-2}	1.296×10^{-2}
0.10	NoEQ	4.784×10^{-1}	4.776×10^{-1}	4.792×10^{-1}
0.10	LS-ZF	4.796×10^{-1}	4.789×10^{-1}	4.804×10^{-1}
0.10	E2E	4.554×10^{-1}	4.546×10^{-1}	4.562×10^{-1}
0.10	Hybrid	4.688×10^{-1}	4.680×10^{-1}	4.695×10^{-1}

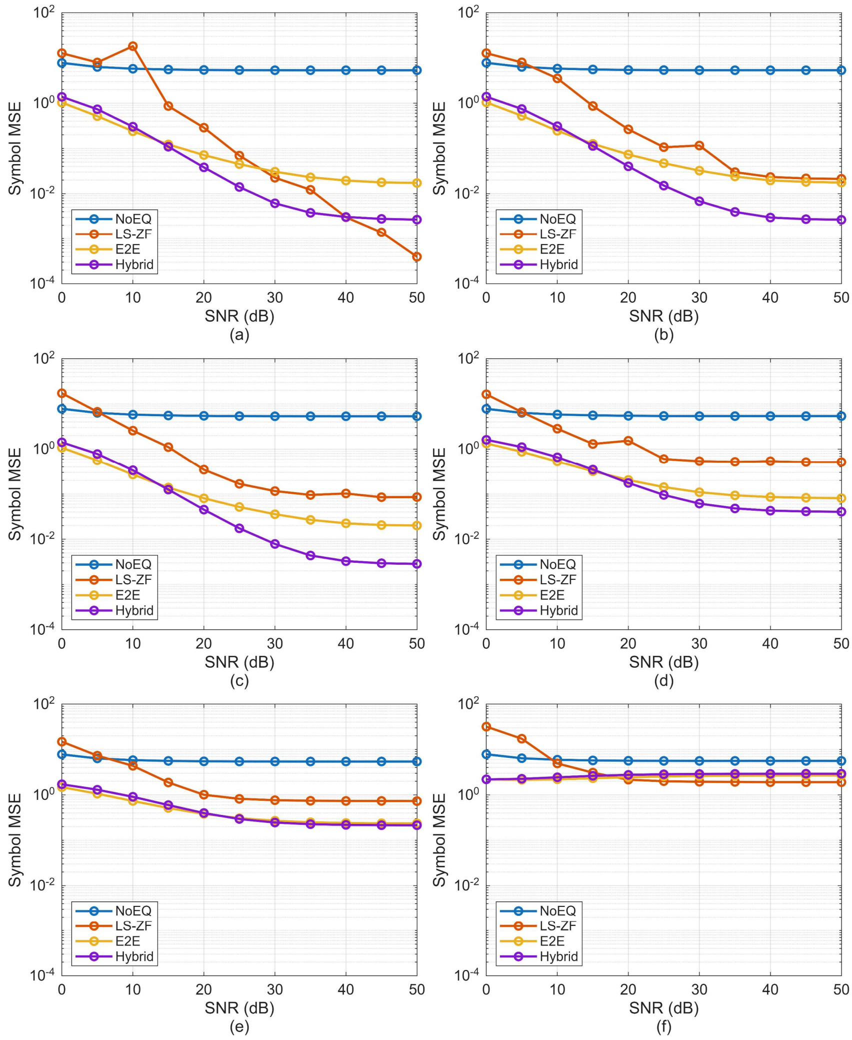

Fig. 4. Symbol MSE versus SNR under the 3GPP TR 38.901 CDL-A channel at 60 GHz for six normalized CFO values: (a) $\epsilon = 0$, (b) $\epsilon = 0.01$, (c) $\epsilon = 0.02$, (d) $\epsilon = 0.05$, (e) $\epsilon = 0.06$, and (f) $\epsilon = 0.10$.

F. EVM Trends: Constellation Quality Under CFO

EVM captures normalized RMS constellation distortion and is especially useful for diagnosing residual phase and frequency impairments. Fig. 5 reports EVM (%) versus SNR across the reported CFO values.

The EVM trends are consistent with the symbol-MSE results. Under low-to-moderate CFO values, the hybrid detector improves constellation fidelity relative to the E2E detector and can substantially reduce residual distortion after LS equalization. At 50 dB and $\epsilon = 0.05$, LS-ZF has an EVM of 50.58%, while the hybrid detector has an EVM of 12.96%, as shown in Fig. 5(d). This indicates that the hybrid correction stage reduces residual constellation error even though its BER remains worse than LS-ZF at the same operating point.

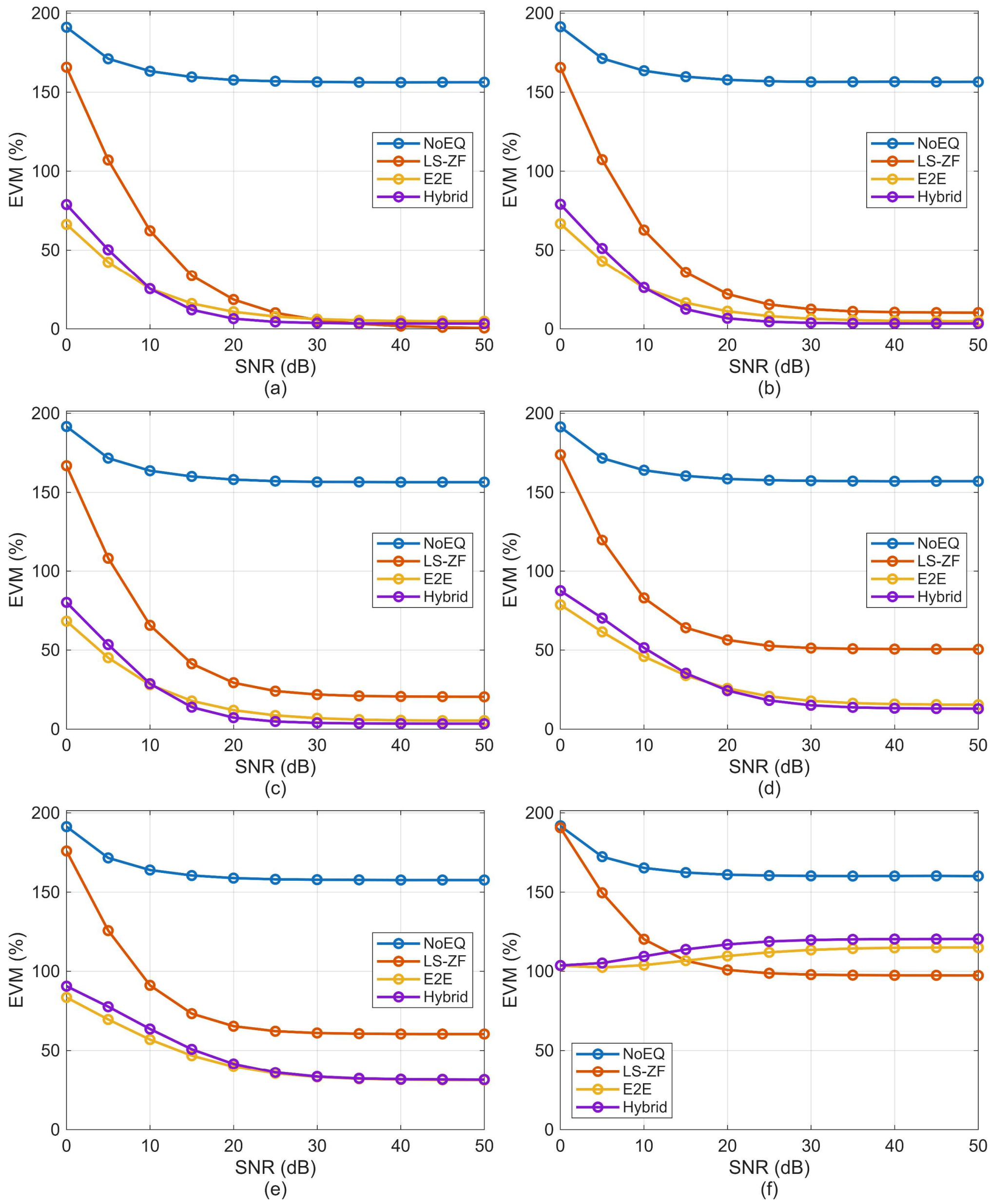

Fig. 5. EVM versus SNR under the 3GPP TR 38.901 CDL-A channel at 60 GHz for six normalized CFO values: (a) $\epsilon = 0$, (b) $\epsilon = 0.01$, (c) $\epsilon = 0.02$, (d) $\epsilon = 0.05$, (e) $\epsilon = 0.06$, and (f) $\epsilon = 0.10$.

The distinction between EVM and BER is important. BER measures only whether a symbol crosses a decision boundary, whereas EVM measures the distance of the detected symbols from their ideal constellation locations. Therefore, the hybrid detector's advantage is best interpreted as an uncoded symbol fidelity gain rather than as a consistent hard-decision BER gain. At stronger CFO values, especially $\epsilon = 0.10$, the EVM of all detectors becomes large, as shown in Fig. 5(f), confirming that the evaluated receivers are not robust to severe out-of-distribution CFO.

G. Discussion: Validation RMSE, Decision Boundaries, and CFO Generalization

The results show that validation RMSE alone is not a sufficient predictor of communication performance. Although the E2E model obtained a lower validation

RMSE than the hybrid model during training, it produced worse BER, MSE, and EVM across much of the evaluated range. This disconnect occurs because the regression loss treats symbol-coordinate errors continuously, whereas BER depends on whether the final estimate crosses a QPSK decision boundary. A model can reduce average coordinate error on the validation set while still producing more decision-boundary crossings under specific channel and impairment conditions.

The feature representation also contributes to this behavior. The E2E detector receives the full raw frequency-domain frame and must implicitly learn channel estimation, equalization, CPE handling, CFO-induced distortion behavior, and symbol detection. This richer input is not necessarily easier to use because it contains pilot, data, channel, and impairment effects entangled in the same feature vector. By contrast, the hybrid detector receives a structured, model-assisted feature comprising the LS channel estimate and the LS-equalized data symbol. The DNN therefore operates on an input in which part of the channel structure has already been exposed by the LS front end, allowing the learned stage to focus on residual correction rather than learning the full receiver mapping from raw samples alone.

The CFO sweep further clarifies the operating range of the detectors. Within low-to-moderate CFO values, LS-ZF remains the strongest BER reference and the hybrid detector remains close in BER while often improving MSE and EVM. However, the performance degradation at $\epsilon = 0.06$ and especially $\epsilon = 0.10$ shows that the learned receivers do not automatically generalize beyond the CFO augmentation range $[-0.05, 0.05]$. Therefore, the hybrid detector should not be interpreted as a universal solution to CFO-impaired OFDM detection. Rather, the results indicate that a structured LS + DNN receiver is more reliable than a direct E2E replacement within the evaluated training and testing regime.

H. Comparison with Existing Approaches and Solutions

The present results are consistent with the broader OFDM deep learning literature: receiver structure remains important. Ye *et al.* [10] showed that a fully connected regression DNN can learn OFDM detection under simulated conditions, but the current results indicate that the same type of simple E2E mapping is less reliable when evaluated under the 3GPP TR 38.901 CDL-A model at 60 GHz with explicit phase-related impairments. By contrast, the hybrid LS + DNN result aligns more closely with model-driven receivers such as ComNet [11] and with the model-driven learning perspective in Ref. [13], where deep learning complements rather than replaces the conventional receiver chain.

These findings are also consistent with comparative studies showing that deep learning does not uniformly dominate classical or iterative methods across all SNR and impairment regimes [14]. In the present case, LS-ZF remains a strong BER baseline, while the hybrid method provides a more targeted gain in residual MSE and EVM. Compared with higher-capacity architectures such as DeepRx [12], this study should therefore be interpreted as a controlled evaluation of where a simple fully connected DNN is useful, not as a state-of-the-art end-to-end replacement, but as a structured post-equalization refinement stage.

I. Overall Interpretation

Taken together, the results indicate that LS-ZF remains a strong BER baseline under TR 38.901 CDL-A at 60 GHz. The hybrid LS + DNN detector is most valuable as a post-equalization refinement stage that can improve uncoded symbol-fidelity metrics under low-to-moderate CFO. However, its gain does not consistently extend to BER and does not hold under severe out-of-distribution CFO.

V. Conclusion

This paper evaluated CFO-aware OFDM detection under the 3GPP TR 38.901 CDL-A channel at 60 GHz using four receiver configurations: NoEQ, LS-ZF, an E2E regression DNN, and a hybrid LS + DNN detector. The study incorporated frame-wise CPE and deterministic normalized CFO, with pilot-based phase compensation applied at the receiver. Performance was measured using BER, symbol MSE, EVM, receiver runtime, and confidence intervals over an expanded CFO sweep.

The results lead to three main conclusions. First, classical LS-ZF remains the strongest BER baseline in the evaluated setting. It performs especially well at low-to-moderate CFO values and provides a difficult reference for learning-based methods to surpass in hard-decision BER. Second, the fully connected E2E detector is less reliable than the structured alternatives, showing clear high-SNR floors and weaker generalization under CFO. Third, the hybrid LS + DNN detector is best interpreted as a post-equalization refinement stage. It remains BER-competitive with LS-ZF under low-to-moderate CFO values and improves symbol-fidelity metrics in several CFO-impaired cases, but it does not consistently improve BER.

The expanded CFO sweep also identifies an important robustness boundary. The DNNs were trained with CFO augmentation in $[-0.05, 0.05]$, and all receivers degrade substantially when tested at $\epsilon = 0.10$. This outcome indicates that a stronger CFO mismatch requires either broader CFO-aware training, explicit synchronization correction, or more advanced model-driven receiver designs.

These findings suggest that, for the evaluated OFDM scenario, deep learning is more effective when used with a communications-domain structure than as a direct end-to-end replacement. Thus, the hybrid gain should be interpreted primarily as an uncoded symbol-fidelity improvement.

Beyond physical-layer detection, the proposed evaluation is also relevant to software-defined 5G/6G Internet of Vehicles (IoV) systems, where adaptive resource management is needed to support multimedia services under energy, scalability, and mobility constraints [26]. A future direction is to integrate the hybrid LS + DNN detector into an SDN-controlled IoV framework in which a higher-layer PID-based controller adjusts receiver operation, such as DNN activation, inference frequency, equalization mode, or synchronization margin, based on BER, EVM, receiver load, and vehicle-speed-dependent channel variation. This approach would connect the present CFO-aware physical-layer evaluation with adaptive, energy-efficient beyond-5G vehicular communication systems.

Several limitations remain. The present work used a simple fully connected DNN, a fixed two-symbol OFDM frame, one CDL profile, zero Doppler, QPSK modulation, and deterministic CFO with frame-wise CPE rather than stochastic Wiener phase noise. Future work should evaluate Doppler-varying channels, stochastic oscillator phase noise, additional CDL profiles, higher-order modulation, coded performance, and more advanced model-driven architectures such as ComNet- or DeepRx-like receivers. It would also be useful to train over wider CFO distributions and test whether improved MSE/EVM can translate into practical BER or throughput gains under higher-order modulation.

Conflict of Interest

The authors declare no conflict of interest.

Author Contributions

Noever Q. Saile conducted the methodology, software implementation, simulations, validation, formal analysis, investigation, and original draft preparation; Lawrence Materum contributed to conceptualization, methodology, supervision, and manuscript review and editing. Both authors approved the final version of the manuscript.

Funding

This work was supported by the De La Salle University, Manila, Philippines, and the Department of Science and Technology, Engineering Research and Development for Technology (DOST-ERDT).

References

[1] R. D. J. V. Nee and R. Prasad, *OFDM for Wireless Multimedia Communications*, Boston: Artech House, 2000.
[2] V. Pollet, M. V. Bladel, and M. Moeneclaey, "BER sensitivity of OFDM systems to carrier frequency offset and Wiener phase noise," *IEEE Transactions on Communications*, vol. 43, no. 2, pp. 191–193, 1995.
[3] S. Wu and Y. B. Ness, "OFDM systems in the presence of phase noise: Consequences and solutions," *IEEE Transactions on Communications*, vol. 52, no. 11, pp. 1988–1996, 2004.
[4] D. Petrovic, W. Rave, and G. Fettweis, "Effects of phase noise on OFDM systems with and without PLL," *IEEE Transactions on Communications*, vol. 55, no. 8, pp. 1607–1616, 2007.
[5] M. R. Khanzadi, R. Krishnan, D. Kuylenstierna, and T. Eriksson, "Oscillator phase noise and small-scale channel fading in higher frequency bands," in *Proc. 2014 IEEE GlobeCom Workshops (GC Wkshps)*, 2014, pp. 410–415.
[6] T. S. Rappaport, S. Sun, R. Mayzus, H. Zhao, Y. Azar, K. Wang, G. N. Wong, J. K. Schulz, M. Samimi, and F. Gutierrez, "Millimeter wave mobile communications for 5G cellular: It will work!" *IEEE Access*, vol. 1, pp. 335–349, 2013.
[7] Z. Qin, H. Ye, G. Y. Li, and B. H. F. Juang, "Deep learning in physical layer communications," *IEEE Wireless Communications*, vol. 26, no. 2, pp. 93–99, 2019.
[8] H. Huang, S. Guo, G. Gui, Z. Yang, J. Zhang, H. Sari, and F. Adachi, "Deep learning for physical-layer 5G wireless techniques: Opportunities, challenges and solutions," *IEEE Wireless Communications*, vol. 27, no. 1, pp. 214–222, 2020.
[9] T. J. O'Shea and J. Hoydis, "An introduction to deep learning for the physical layer," *IEEE Transactions on Cognitive Communications and Networking*, vol. 3, no. 4, pp. 563–575, 2017.
[10] H. Ye, G. Y. Li, and B. H. Juang, "Power of deep learning for channel estimation and signal detection in OFDM systems," *IEEE Wireless Communications Letters*, vol. 7, no. 1, pp. 114–117, 2018.
[11] X. Gao, S. Jin, C.-K. Wen, and G. Y. Li, "ComNet: Combination of deep learning and expert knowledge in OFDM receivers," *IEEE Communications Letters*, vol. 22, no. 12, pp. 2627–2630, 2018.
[12] M. Honkala, D. Korpi, and J. M. J. Huttunen, "DeepRx: Fully convolutional deep learning receiver," *IEEE Transactions on Wireless Communications*, vol. 20, no. 6, pp. 3925–3940, 2021.
[13] H. He, S. Jin, C.-K. Wen, F. Gao, G. Y. Li, and Z. Xu, "Model-driven deep learning for physical layer communications," *IEEE Wireless Communications*, vol. 26, no. 5, pp. 77–83, 2019.
[14] H. Ju, H. Zhang, L. Li, X. Li, and B. Dong, "A comparative study of deep learning and iterative algorithms for joint channel estimation and signal detection in OFDM systems," *Signal Processing*, vol. 223, 109554, 2024.
[15] H. Hashempoor and W. Choi, "Deep learning-based data-assisted channel estimation and detection," *IEEE Transactions on Machine Learning in Communications and Networking*, vol. 3, pp. 534–551, 2025.
[16] 3GPP. Study on channel model for frequencies from 0.5 to 100 GHz. ETSI TR 138.901 V16.1.0, Nov. 2020, Release 16. [Online]. Available: https://www.etsi.org/deliver/etsi_tr/138900_138999/138901/16.01.00_60/tr_138901v160100p.pdf
[17] Z. Wang, S. Wei, L. Zou, F. Liao, W. Lang, and Y. Li, "Deep-learning-based carrier frequency offset estimation and its cross-evaluation in multiple-channel models," *Information*, vol. 14, no. 2, 98, 2023.
[18] X. Li, Y. Wang, X. Zhao, K. Xu, H. Dai, Q. Zhang, Y. Zhang, and J. Wang, "TrsNet: A TRS-based deep learning network for carrier frequency offset estimation in 5G system," *Telecommunication Systems*, vol. 88, 2, 2025.
[19] H. Wu, Z. Chen, Z. Liu, X. Geng, Y. Zhao, and Z. Liu, "CRS-based joint CFO and channel estimation using deep learning in OFDM-based vehicular communication systems," *IEEE Transactions on Wireless Communications*, vol. 24, no. 5, pp. 3882–3893, 2025.
[20] M. Soltani, V. Pourahmadi, A. Mirzaei, and H. Sheikhzadeh, "Deep learning-based channel estimation," *IEEE Communications Letters*, vol. 23, no. 4, pp. 652–655, 2019.
[21] X. Yi and C. Zhong, "Deep learning for joint channel estimation and signal detection in OFDM systems," *IEEE Communications Letters*, vol. 24, no. 12, pp. 2780–2784, 2020.
[22] C. Y. Wu, Y. K. Lin, C. K. Wu, and C.-H. Lee, "Deep learning-based end-to-end design for OFDM systems with hardware impairments," *IEEE Open Journal of the Communications Society*, vol. 4, pp. 2468–2482, 2023.
[23] X. Lin, Y. Shen, and C. Jiang, "A model-driven deep learning-based receiver for OFDM system with carrier frequency offset," *IEEE Communications Letters*, vol. 28, no. 4, pp. 813–817, 2024.
[24] J. Pihlajasalo, D. Korpi, M. Honkala, J. M. J. Huttunen, T. Riihonen, J. Talvitie, A. Brihuega, M. A. Uusitalo, and M. Valkama, "Deep learning OFDM receivers for improved power efficiency and coverage," *IEEE Transactions on Wireless Communications*, vol. 22, no. 8, pp. 5518–5535, 2023.
[25] M. Shammaa, M. Mashaly, and A. El-mahdy, "The use of deep learning techniques in OFDM receivers for 5G NR: A survey," *Procedia Computer Science*, vol. 231, pp. 32–39, 2024.
[26] A. Montazerolghaem, "Energy-efficient software-defined 5G/6G multimedia IoV: PID controller-based approach," *IEEE Transactions on Vehicular Technology*, vol. 75, no. 6, pp. 11621–11633, 2026.